Progerin and telomere dysfunction collaborate to trigger cellular senescence in normal human fibroblasts

Kan Cao,[1,2] Cecilia D. Blair,[1] Dina A. Faddah,[1] Julia E. Kieckhaefer,[2] Michelle Olive,[1] Michael R. Erdos,[1] Elizabeth G. Nabel,[1] and Francis S. Collins[1]

[1]Genome Technology Branch, National Human Genome Research Institute, NIH, Bethesda, Maryland, USA.
[2]Department of Cell Biology and Molecular Genetics, University of Maryland, College Park, Maryland, USA.

Hutchinson-Gilford progeria syndrome (HGPS), a devastating premature aging disease, is caused by a point mutation in the lamin A gene (*LMNA*). This mutation constitutively activates a cryptic splice donor site, resulting in a mutant lamin A protein known as progerin. Recent studies have demonstrated that progerin is also produced at low levels in normal human cells and tissues. However, the cause-and-effect relationship between normal aging and progerin production in normal individuals has not yet been determined. In this study, we have shown in normal human fibroblasts that progressive telomere damage during cellular senescence plays a causative role in activating progerin production. Progressive telomere damage was also found to lead to extensive changes in alternative splicing in multiple other genes. Interestingly, elevated progerin production was not seen during cellular senescence that does not entail telomere shortening. Taken together, our results suggest a synergistic relationship between telomere dysfunction and progerin production during the induction of cell senescence, providing mechanistic insight into how progerin may participate in the normal aging process.

Introduction

Cellular senescence, the finite division capacity of normal somatic cells in vitro, has long been used as a cellular model for understanding mechanisms underlying normal aging (1, 2). A popular hypothesis of cellular senescence is that progressive attrition of telomeric DNA results in loss of telomere capping proteins, exposing DNA breaks that activate cell cycle arrest and senescence (3). Telomeres are the specialized structures at the chromosome ends, made up of many kilobases of a simple DNA repeat $(TTAGGG)_n$ bound by a multiprotein complex known as shelterin (4). Telomeres cannot be copied to their extreme termini by DNA polymerase, and so undergo progressive shortening unless elongated by a ribonucleoprotein named telomerase (5, 6). Telomerase is composed of a reverse transcriptase (TERT) and an RNA component (TERC) that serves as a template for telomere elongation (6, 7). In somatic cells lacking telomerase, gradual telomere loss and ultimate senescence are inevitable (8). Consistent with this model, there is a strong association between cell immortalization and persistent telomerase expression (9). Besides telomere shortening, cellular senescence can be triggered by a variety of environmental and intracellular stimuli, including γ-irradiation, oxidative stress, and overexpression of certain oncogenes, such as H-rasV12 (10–12). Moreover, mutations in certain genes, such as lamin A (*LMNA*; accession no. NM_170707), have been linked to premature senescence (13, 14).

LMNA encodes 2 intermediate filament proteins, lamin A and lamin C. Together with lamin B, they form a dynamic meshwork located just inside the nuclear inner membrane, named the nuclear lamina. The lamina provides important mechanical support to the nuclear structure and also influences chromatin organization, gene expression, and DNA replication (15–17). To date, at least 13 human diseases (referred to as the laminopathies) have been associated with the mutations in lamin genes (13). Among them, Hutchinson-Gilford progeria syndrome (HGPS) has received the most attention because of its striking premature aging phenotype, including alopecia, diminished subcutaneous fat, premature atherosclerosis, and skeletal abnormalities. Children with HGPS die at an average age of 12 years, usually from heart attack or stroke (18). The vast majority of HGPS cases are associated with a de novo nucleotide substitution at position 1824 (C→T) in the *LMNA* gene (14, 19). This mutation does not affect the coded amino acid (and is thus generally referred to as G608G), but partially activates a cryptic splice donor site in exon 11 of *LMNA*, leading to the production of a prelamin A mRNA that contains an internal deletion of 150 base pairs (14). This transcript is then translated into a protein known as progerin, which lacks 50 amino acids near the C terminus (14). Indeed, progerin has been found to accumulate in multiple tissues in biopsies from HGPS patients, including skin, tongue, breast, heart, liver, kidney, stomach, bladder, diaphragm, pancreas, spleen, thyroid, adipose tissue, joint cartilage, bone, skeletal muscle, heart, and large and small arteries (20).

The cellular phenotypes in HGPS include blebbing (i.e., abnormal shape) of nuclei, thickening of the nuclear lamina, loss of peripheral heterochromatin, clustering of nuclear pores, and premature senescence (21). Interestingly, prior to developing these obvious nuclear morphological changes, fibroblasts from HGPS patients exhibit broad abnormalities in histone modification patterns (22). HGPS fibroblasts also show global changes in gene expression (23, 24) and a delayed response in DNA-damage repair (25).

Gene transfer experiments have left no doubt that progerin acts as a dominant negative. Progerin expression induces multiple defects during mitosis: cytokinesis delay, abnormal chromosome segregation, and binucleation (26, 27). Several *Lmna* mutant mouse models have been created. A transgenic model carrying the G608G mutated human *LMNA* in a bacterial artificial chromo-

Conflict of interest: The authors have declared that no conflict of interest exists.
Citation for this article: *J Clin Invest.* 2011;121(7):2833–2844. doi:10.1172/JCI43578.

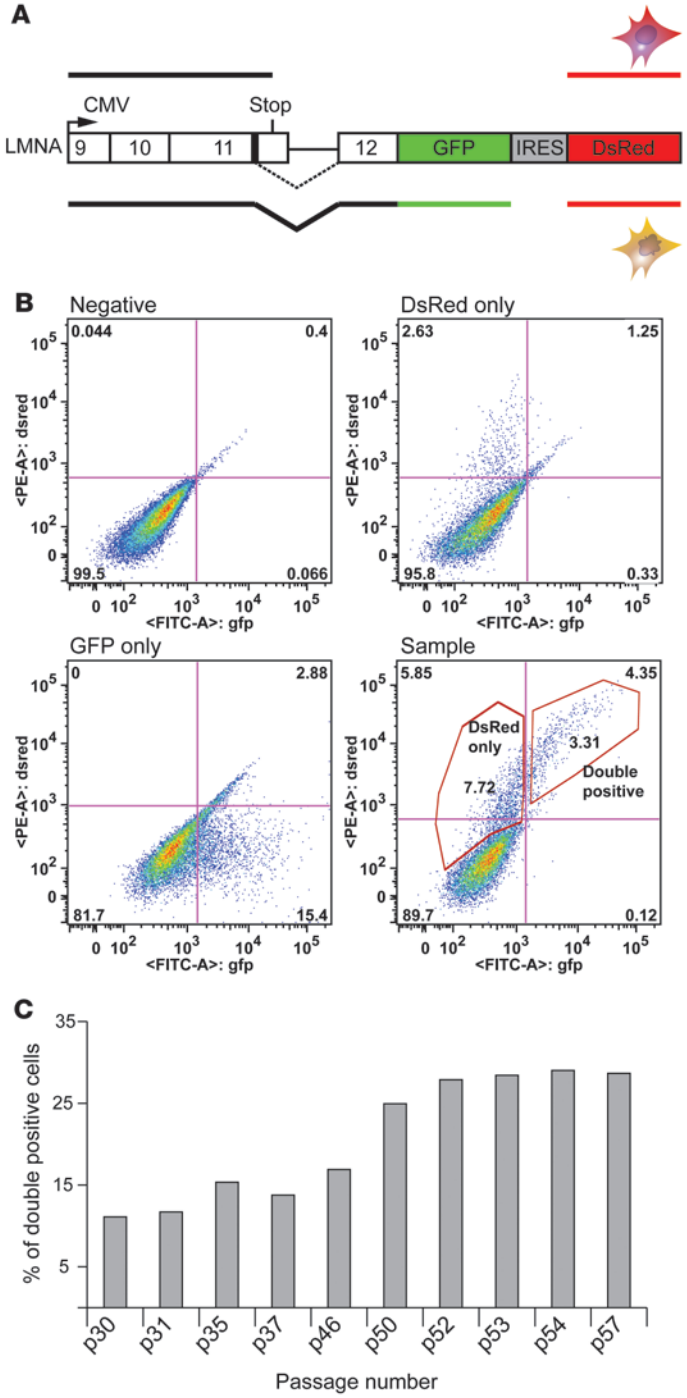

Figure 1
Cellular senescence activates *progerin* transcription. (**A**) Schematic representation of the double-color progerin splicing reporter construct. The cryptic splice site is shown as a solid box in exon 11. (**B**) FACS analysis of fibroblasts from a normal individual (AG06299) transiently transfected with buffer (Negative), the pIRES-DsRed-Expression 2 vector (DsRed only), the pEGFP-N1 vector (GFP only), or the progerin splicing reporter construct (Sample). (**C**) The percentage of cells with activation of the progerin splicing site increased with the number of cell passages. Results from a fibroblast line derived from a normal individual (AG06299) are shown.

some (BAC) shows progressive loss of vascular smooth muscle cells in the medial layer of large arteries, closely resembling the most lethal aspect of the human phenotype (28).

The molecular mechanism of progerin toxicity is at least partially understood. Normal lamin A is farnesylated at its C terminus, and that posttranslational modification is thought to play a role in targeting lamin A to the inner nuclear membrane. But subsequently, the ZMPSTE24 endoprotease cleaves off the last 18 amino acids at the C terminus of lamin A, including the farnesyl tail. This releases lamin A from its membrane anchor and allows it to take its place in the nuclear scaffold (29). The 50–amino acid internal deletion in progerin includes the ZMPSTE24 cleavage site, and thus progerin remains permanently farnesylated (27). Recently, treatment with farnesyl transferase inhibitors (FTIs) has been shown to improve progerin-induced cellular phenotypes in vitro and in several HGPS mouse models (13, 27, 30–34). A clinical trial with an FTI in children with HGPS was initiated in May 2007.

It has always been of great interest to determine the biological relevance of HGPS to normal aging. This interest was heightened by the detection of *progerin* mRNA and progerin protein in cells obtained from healthy individuals, which indicates that the cryptic splice site activated by the HGPS mutation is also capable of being used in the presence of the normal sequence of exon 11 (35). Recently, *progerin* transcripts and progerin were identified in vivo in skin biopsies from healthy individuals, and a recent analysis suggested that *progerin* transcript levels increase in late-passage cells from HGPS patients and parental controls (36, 37).

Using a reporter construct, Scaffidi et al. showed that the normal *LMNA* sequence at G608G could also be used as a weak splice donor to produce progerin in normal individuals (35). We have previously shown that a significant percentage of progerin-positive cells from normal individuals are morphologically abnormal, exhibiting phenotypes that resemble HGPS cells (26). This suggests that activation of progerin expression in normal cells, triggered by some unknown signal, may contribute to senescence.

However, the cause-and-effect relationship between normal aging and progerin production in normal individuals has not been determined. In the present study, we assayed the effects of cellular passage and donor age on the activation of progerin production and found that the cryptic splice donor site that produces progerin is activated in senescent cells. Screening various primary and transformed cell lines revealed an interesting inverse correlation between cell immortalization and *progerin* transcription, and ectopic expression of telomerase in normal fibroblast cells resulted in a significant decrease in progerin production. In addition, we found that progerin production was not induced in telomere-independent, oncogene-driven senescence, further supporting a potential causal relationship between telomere-induced senescence and progerin production. Consistent with this model, we found that elevated levels of progerin were induced in fibroblast cells whose telomeres had been uncapped. With splicing-sensitive exon microarrays, we further showed that extensive changes in alternative splicing of multiple genes, including *LMNA*, occurred as telomeres shortened

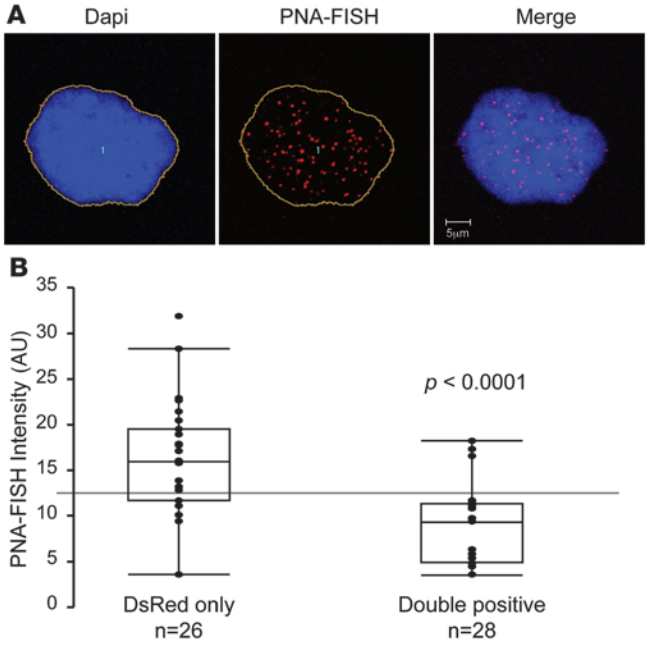

Figure 2

Progerin-expressing cells from normal individuals show signs of senescence. (**A**) An example of the quantitative telomere PNA-FISH analysis of a normal fibroblast cell (HGFDFN168). DNA was stained with DAPI in blue to show the boundary of the nucleus (outlines), and telomere-FISH signals are in red. Scale bar: 5 μm. (**B**) Box plot representation of the absolute fluorescence intensity of the telomere-FISH in double-positive (n = 26) and DsRed-only (n = 28) cells. Each dot represents the absolute fluorescence intensity in 1 tested cell. Box denotes 25th and 75th percentiles; line within box denotes 50th percentile; whiskers denote 9th and 91st percentiles. $P < 0.0001$, double-positive vs. DsRed-only.

and cells approached senescence. Taken together, our findings are suggestive of synergism between telomere damage and progerin production in induction of cellular aging and provide what we believe to be the first genome-wide analysis of the changes in alternative splicing during cell senescence.

Results

Cellular senescence activates progerin production. To elucidate the cause-and-effect relationship between aging and progerin production, we designed a splicing reporter assay that permits observation of the immediate effects of cell passage or donor age on the activation of the progerin cryptic splice donor site. The cryptic splicing reporter originally described by Scaffidi et al. (35) was PCR amplified and subcloned into a bicistronic vector (pIRES-DsRed-Expression 2) (Figure 1A). This 2-color progerin splicing reporter was then transiently transfected into normal fibroblast cells. In this assay, all transfected cells expressed red fluorescence protein, and cells using the cryptic splice site also expressed GFP (Supplemental Figure 1, A and B; supplemental material available online with this article; doi:10.1172/JCI43578DS1). At 96 hours after transfection, we sorted those fibroblasts with fluorescence-activated cell sorting (FACS) analysis and quantified 2 subpopulations (Figure 1B and Supplemental Figure 1A): the fraction positive for both GFP and DsRed, consisting of transfected cells that had activated the cryptic splice site in *LMNA* (referred to herein as *double-positive*), and the fraction positive for DsRed only, containing the transfected cells that did not use the cryptic splice (referred to herein as *DsRed-only*). To examine the effect of cellular passage and donor age, we performed the reporter assay in 6 independent primary fibroblast lines, derived from healthy donors ranging 10–92 years in age, at increasing cellular passages. Percent double-positive cells relative to total DsRed cells was used as an indicator of the progerin splicing activity and plotted against cell passage and donor age. In all tested cell lines, we consistently observed that double-positive cell percentage increased with cell passage (Figure 1C and Supplemental Figure 2), which suggests that cellular senescence correlates with activation of progerin splicing. Furthermore, in agreement with previous reports (35, 36, 38, 39), we did not observe an obvious correlation of progerin production with donor age (Supplemental Figure 2).

Progerin-expressing cells from normal individuals show signs of senescence. To gain mechanistic insights into the activation of the progerin cryptic splice site in cellular aging, we next compared telomere length in the double-positive and DsRed-only subgroups after FACS analysis. The telomeres were labeled using FISH with a peptide nucleic acid probe against telomere repeat sequence (PNA-FISH). The telomere length of each cell was quantified as the total fluorescence intensity from PNA-FISH in each nucleus, which was defined by the DAPI staining of DNA (Figure 2A). We examined 2 normal fibroblast cell lines, AG06299 at passage 35 (p35) and HGFDFN168 at p18. Because both cell lines demonstrated similar results, we showed results only from HGFDFN168. Box plot analysis indicated that the telomeres in the double-positive subgroup were significantly shorter than those in the DsRed-only subgroup from the same cell line ($P < 0.0001$; Figure 2B). Taken together, these results indicate that the progerin-producing double-positive cells define a subpopulation of cells with short telomeres, which suggests a potential connection between telomere erosion and progerin splicing activation.

Immortalized cells suppress progerin production. To further test the connection between progressive telomere shortening and progerin production, we measured the amount of *progerin* mRNA in immortalized cancer cells with stable telomeres as a result of telomerase expression as well as in primary cells lacking telomerase expression. A RT-PCR assay with progerin- or lamin A–specific primers was designed to assess relative use of the endogenous lamin A cryptic splice site (Figure 3A). Paired with a forward primer at the exon 7–8 junction, these primers specifically amplified truncated progerin or lamin A products with the expected sizes. A high level of specificity was demonstrated using in vitro–purified cDNAs (Supplemental Figure 3). DNA sequencing verified the identities of these PCR products (data not shown). We tested a total of 16 cell lines, including 12 primary cell lines derived from 3 cell types (fibroblasts, aortic SMCs, and B lymphocytes) and 4 immortalized cell lines from various telomerase-positive cancers (Figure 3B). Consistent with previous reports (40), quantitative RT-PCR (qRT-PCR) analysis revealed substantial variation in *LMNA* expression in different cell types, with the lowest expression found in B lymphocytes (15-fold less than fibroblasts; data not shown). To directly compare the level of *progerin* mRNA among these different types of cells, we normalized the amount of *progerin* mRNA to the *LMNA* mRNA in each cell line. Interestingly, we found that *progerin* mRNA was essentially absent in immortalized cells with stable telomeres (Figure 3B).

Next, we examined how changes in telomere length would influence progerin production. We studied 2 human TERT–immortalized normal fibroblast cell lines, hTERT-HGFDFN090 and

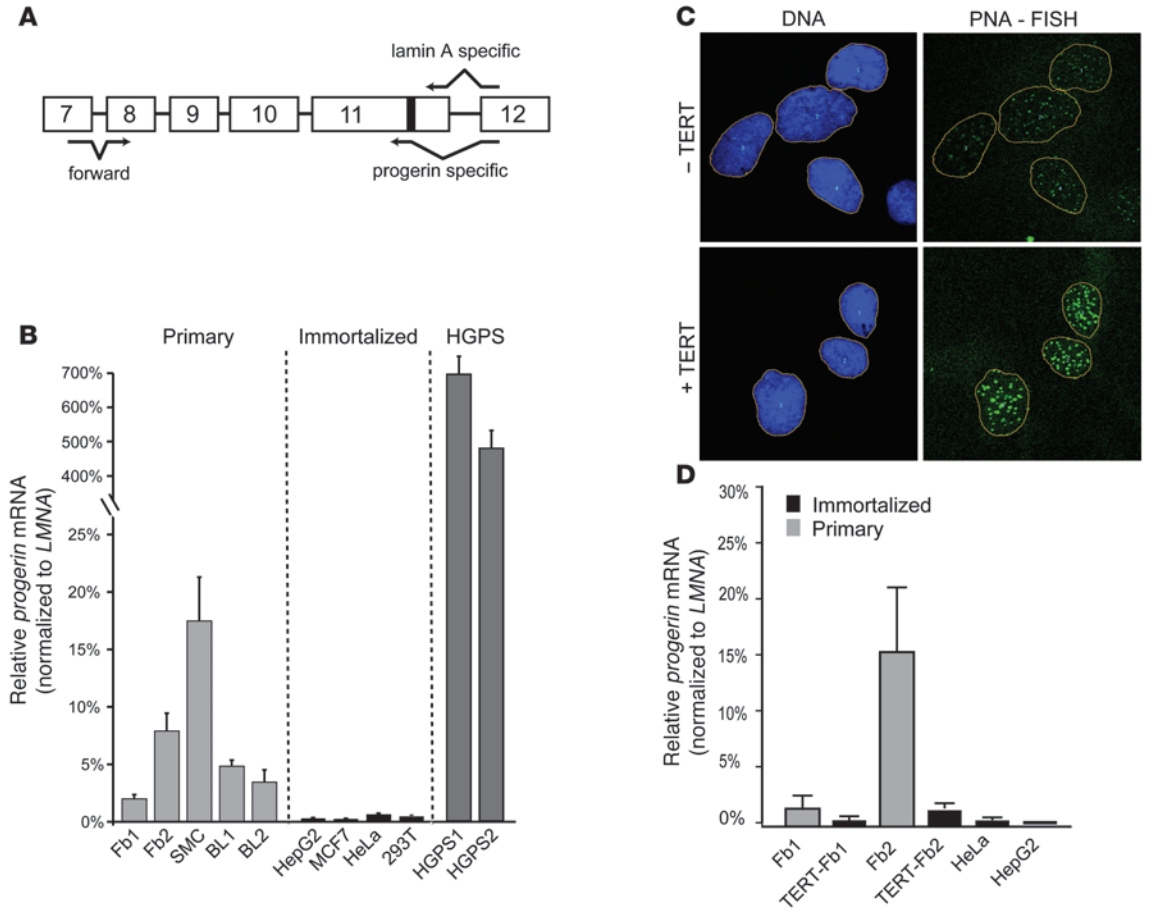

Figure 3

Immortalized cells suppress *progerin* transcription. (**A**) Schematic representation of the positions of progerin- or lamin A– specific primers used for RT-PCR analysis. (**B**) qRT-PCR. Primary lines included normal fibroblast cell lines HGFDFN168 and HGFDFN090 (Fb1 and Fb2, respectively); human aortic SMC line; and B lymphocyte lines AG09393 and AG11659 (BL1 and BL2, respectively). HGPS fibroblast lines were HGADFN167 and HGADFN003 (HGPS1 and HGPS2, respectively). 4 immortalized lines of indicated cell types are also shown. qRT-PCR showed more *progerin* mRNA than *LMNA* mRNA in HGPS cell lines, which was an artifact caused by the difference in priming efficiency of progerin-and lamin A–specific primers (see Supplemental Figure 4C). (**C**) Representative images of quantitative telomere PNA-FISH analysis of human TERT–immortalized (+TERT) and primary (–TERT) fibroblast cells (AG09838, p8). DNA was stained with DAPI in blue to show the boundary of the nucleus (outlines), and telomere-FISH signals are in green. (**D**) qRT-PCR analysis of the total *progerin* mRNA amount in normal and human TERT–immortalized cell lines with progerin-specific primers. The relative expression values for *progerin* were normalized to the mean values of endogenous *LMNA*. HeLa and 293T lines are shown as controls.

hTERT-AG09838, and their parent cells. qRT-PCR analysis with human TERT primers confirmed the presence of *TERT* mRNA in the immortalized fibroblast cells, whereas no *TERT* mRNA was detected in their nonimmortalized counterparts because of its extremely low amount in differentiated primary fibroblasts (data not shown). In addition, quantitative telomere PNA-FISH analysis demonstrated that stable infection of human TERT resulted in elongated telomeres (Figure 3C and Supplemental Figure 4). Consistent with our finding in immortalized cancer cells, we found that the ectopic expression of telomerase in normal fibroblasts led to significant downregulation in progerin production: *progerin* mRNA decreased 3- and 10-fold in hTERT-AG08398 and hTERT-HGFDFN090 fibroblasts, respectively, compared with their nonimmortalized passage-matched counterparts (Figure 3D). Therefore, we concluded that forced elongation of telomeres in primary fibroblast cells leads to suppression of progerin production. Together, our data demonstrated an inverse correlation between telomerase expression (cell immortalization) and progerin production and suggested that telomeres serve as the upstream signals in regulating progerin production.

Progerin production is not altered in telomere-independent premature cellular senescence. To examine whether progerin splicing is activated in cellular senescence that does not entail telomere shortening, we analyzed progerin production in premature senescence induced by oncogenic ras (12). We chose 2 well-characterized normal fibroblast lines, AG08470 and HGFDFN168, and introduced an activated ras allele (H-rasV12) to those cells using the pBABE retrovirus, as previously described (12). The vector coexpresses a puromycin-resistant gene that allows selection for transduced cells in 4–5 days. After selection, those cells were grown in media without puromycin for an additional 6 days. Expression of H-rasV12 induced morphological changes in both normal fibroblast cell

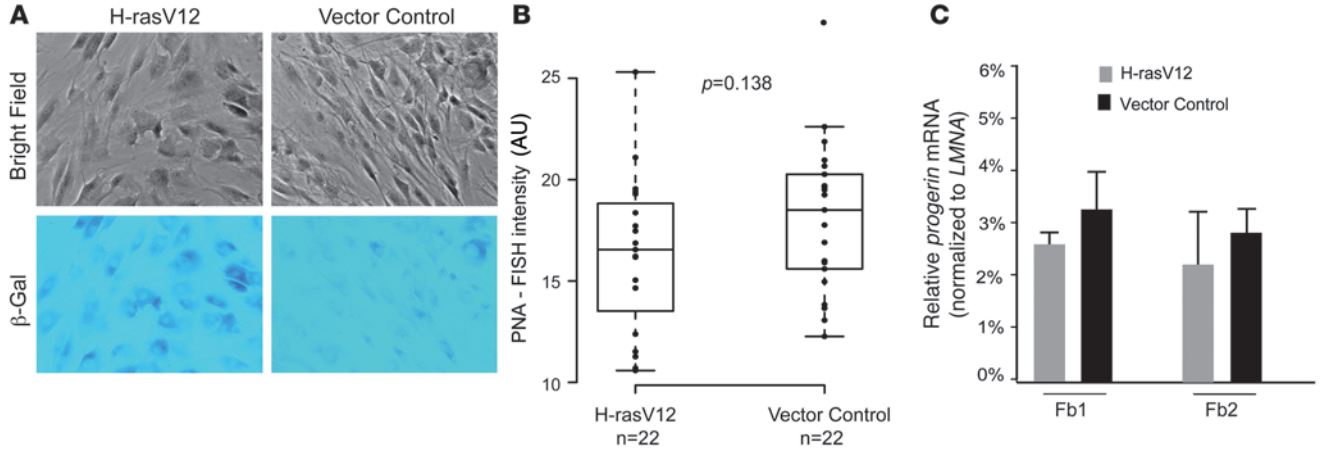

Figure 4
Progerin production is not increased in oncogene ras–induced premature cellular senescence. (**A**) Vector control and H-rasV12–infected AG08470 cells stained for SA–β-gal activity at day 6 after puromycin selection. (**B**) Box plot representation of the quantitative telomere PNA-FISH in the vector control or H-rasV12 transfected AG08470 cells (P = 0.138; n = 22 per group). Box denotes 25th and 75th percentiles; line within box denotes 50th percentile; whiskers denote 9th and 91st percentiles. (**C**) qRT-PCR analysis of total *progerin* mRNA in H-rasV12– or control-infected normal fibroblast cells with progerin-specific primers. Relative expression values for *progerin* were normalized to the mean values of endogenous *LMNA*. Fb1 and Fb2, replicates performed in AG08470 and HGFDFN168, respectively, at p14.

lines. A substantial portion of H-rasV12–transduced cells became flat and enlarged and exhibited increased SA–β-gal activity (Figure 4A). No changes in morphology were detected in cells transduced with vector control (Figure 4A). Consistent with previous studies (12), quantitative telomere PNA-FISH analysis demonstrated no obvious changes in telomere length in H-rasV12–induced cells compared with that in control vector–induced cells (Figure 4B). Importantly, although the morphological features of H-rasV12–induced cells closely resembled cells that have passed their proliferative capacity and become senescent, qRT-PCR analysis indicated no upregulation of progerin production in either cell line tested (Figure 4C). In addition, we found no significant upregulation of *progerin* mRNA production in the premature senescent cells that had been induced by treatment with 0.5 mM sodium butyrate, a histone deacetylase inhibitor (41), for 2 weeks (data not shown). Together, these data suggest that upregulation of progerin production is not a common feature for all types of senescence, but appears specific for telomere-driven senescence.

Fibroblast cells from dyskeratosis congenita patients carrying a heterozygous null mutation in human TERT produce more progerin. To further test the hypothesis that short telomeres activate progerin production in senescent cells, we used 2 fibroblast lines, JH-1 and JH-2, derived from patients with dyskeratosis congenita (DC) (42). These cells carry a heterozygous loss-of-function mutation (K902N) in exon 11 of *TERT* that results in haploinsufficiency of telomerase and accelerated telomere shortening (42). DNA sequencing verified the presence of K902N in both DC fibroblast lines (Supplemental Figure 5). Quantitative telomere PNA-FISH analysis confirmed accelerated telomere loss during cellular senescence in these DC cells compared with passage-matched normal fibroblasts (P < 0.0001; Figure 5A). Using qRT-PCR on cells at p12–p15, we found a more than 2-fold increase in progerin production in these DC fibroblasts compared with normal passage-matched control cells (P = 0.013; Figure 5B). Interestingly, both JH-1 and JH-2 cells exhibited a more than 2-fold increase in cell blebbing (Figure 5, C and D; see Supplemental Figure 6 for passage-matched normal fibroblast control), reminiscent of the hallmark cellular phenotype in HGPS. In addition, we noted a significant increase in JH-1 and JH-2 cells containing micronuclei (small unincorporated chromosome fragments; Figure 5, C and D), potentially caused by prior defects in cell division, which has also been reported in HGPS cells (26, 27). Immunostaining of the JH-1 and JH-2 cells with an anti-progerin antibody revealed positive progerin staining inside micronuclei in those abnormal cells (Figure 5E). The specificity of the anti-progerin antibody was verified using immunostaining in HeLa cells expressing either GFP-progerin or GFP–lamin A (Supplemental Figure 7). Interestingly, we observed positive cytoplasmic signals of progerin in a small percentage of DC cells (Figure 5E), which contrasts with the predominant nuclear lamina localization of WT lamin A and lamin C. Our data in DC cells provide further support for a model in which short telomeres act as an upstream signal to activate progerin production in primary fibroblast cells.

Fibroblasts expressing TRF2$^{\Delta B\Delta M}$ show increased progerin production. To address further the effect of telomere-directed senescence on progerin production, we used TRF2 inhibition as a tool to induce immediate telomere dysfunction in normal cells. TRF2 is a major component of the telomere-capping complex, shelterin (4). When TRF2 is dislodged from telomeres by a dominant-negative allele (TRF2$^{\Delta B\Delta M}$), a fraction of chromosome ends lose their protection, leading to a growth arrest that is indistinguishable from replicative senescence (43). We infected normal human fibroblasts with retroviruses expressing TRF2$^{\Delta B\Delta M}$ or WT TRF2. Cells were kept under puromycin-containing medium for 5 days before being used for analysis. qRT-PCR analysis with progerin- and lamin A–specific primer pairs indicated no significant changes of WT *LMNA* mRNA level, but more than 8-fold upregulation of *progerin* mRNA was observed in TRF2$^{\Delta B\Delta M}$-expressing cells compared with control cells (Figure 6, A and B). Western blotting analysis with the anti-progerin antibody revealed a distinct band corresponding to progerin in cells infected with TRF2$^{\Delta B\Delta M}$, but not in control cells infected with

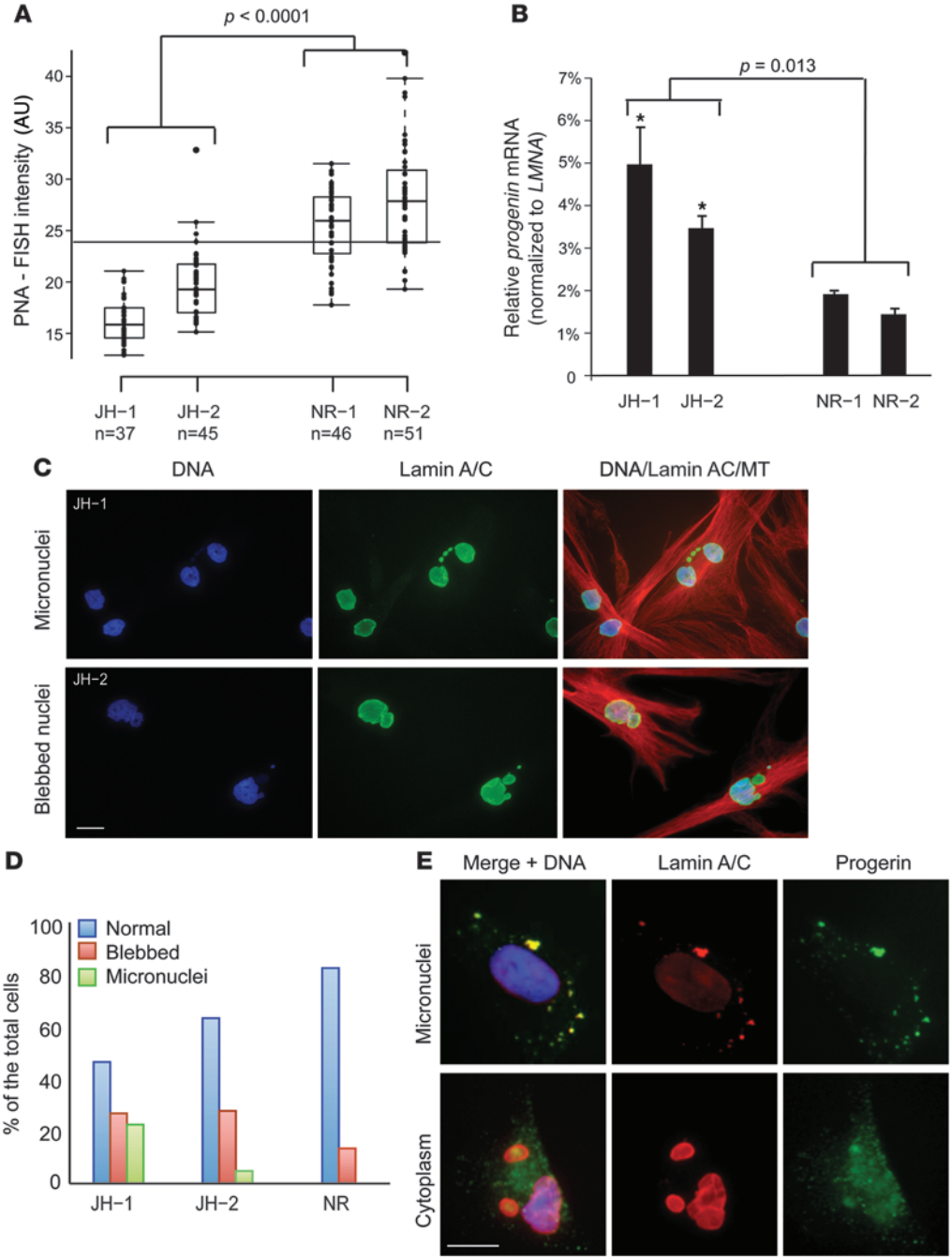

Figure 5

Progerin production is more abundant in passage-matched DC fibroblasts that carry a TERT mutation. (**A**) Box plot representation of the quantitative telomere PNA-FISH in JH-1 and JH-2. JH-1 and JH-2 had significantly shorter telomeres compared with passage-matched normal fibroblast controls ($P < 0.0001$). All cell lines were analyzed at p12–p15. NR1 and NR2, normal fibroblast controls HGFDFN168 and HGFDFN090, respectively, at p14. *n* is indicated for each group. Box denotes 25th and 75th percentiles; line within box denotes 50th percentile; whiskers denote 9th and 91st percentiles. (**B**) qRT-PCR analysis of *progerin* mRNA in JH-1 and JH-2 cells. The relative expression values for *progerin* were normalized to the mean values of *LMNA*. Significantly greater amounts of *progerin* were observed in p12 JH-1 and p15 JH-2 cells, which have accelerated telomere shortening ($P = 0.013$, p12 JH-1 and p15 JH-2 vs. p14 NR-1 and p14 NR-2). (**C**) Immunofluorescence of JH-1 and JH-2 fibroblast cells with anti-lamin A/C antibody (green) and anti–α-tubulin (MT; red) antibody. DNA is labeled with DAPI in blue. (**D**) Quantification of nuclear blebbing and micronuclei in p12 JH-1 and p15 JH-2 cells. A normal fibroblast (NR; AG08470 at p14) was used as a control. (**E**) Immunostaining with anti-progerin antibody in selected DC cells. DNA is stained with DAPI in blue. Scale bar: 10 μm.

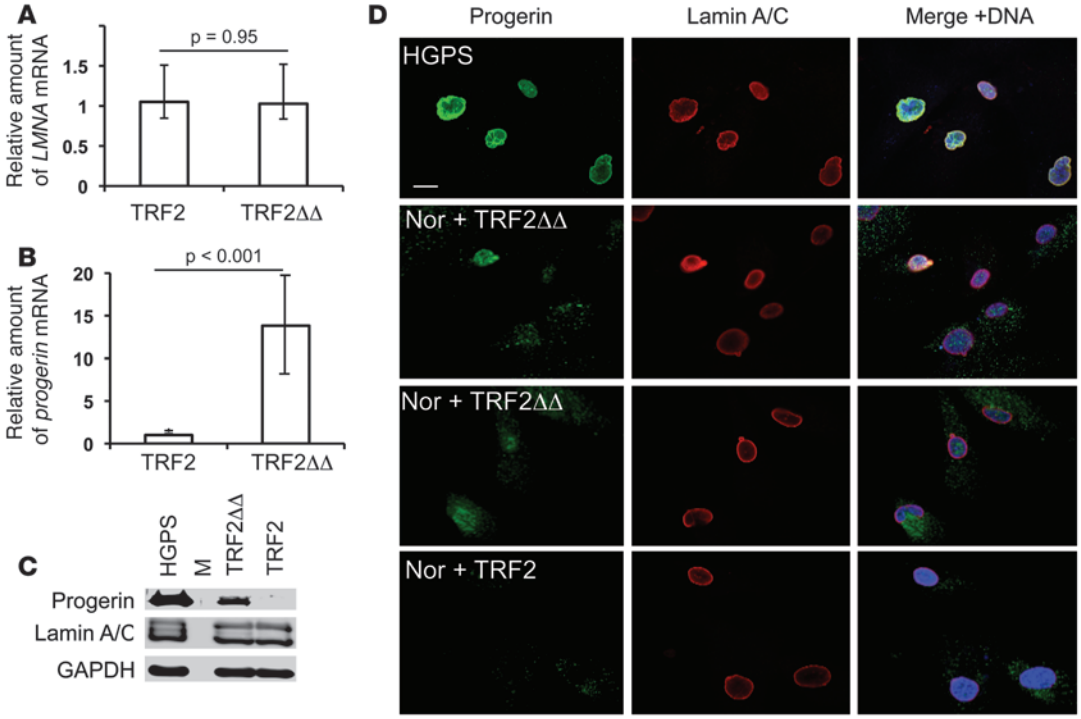

Figure 6
Progerin production is upregulated in cells with uncapped telomeres. (**A** and **B**) qRT-PCR analysis of TRF2 and TRF2$^{\Delta B \Delta M}$ (TRF2ΔΔ) cells with the progerin- or lamin A–specific primer pairs. Amounts of *progerin* (**B**) and *LMNA* (**A**) relative to *ACTB* are shown. (**C**) Western blotting analysis of progerin amount in normal fibroblasts infected with WT TRF2 or TRF2$^{\Delta B \Delta M}$. M, marker lane. (**D**) Immunofluorescence with anti-lamin A/C antibody (red) and anti-progerin (green) antibody. Nor, normal human fibroblasts. Scale bar: 10 μm.

WT TRF2 (Figure 6C). Similarly, immunofluorescence analysis revealed positive progerin staining in the TRF2$^{\Delta B \Delta M}$ cells (Figure 6D). Interestingly, we found that progerin staining in TRF2$^{\Delta B \Delta M}$ cells was quite diffuse in the nucleoplasm and was even seen in the cytoplasm in some cells. This differs with the predominant nuclear lamina localization of WT lamin A/C. We reasoned that the apparent lack of signal from the anti–lamin A/C antibody in the progerin-positive cytoplasm might be just a sensitivity issue, since there is such a large amount of lamin A/C in the nucleus. Indeed, simply by increasing the gain of the signal for lamin A/C, we observed colocalization of signals from anti-progerin and anti–lamin A/C antibodies (Supplemental Figure 8). In summary, these data support the conclusion that uncapped dysfunctional telomeres activate the cryptic splice site in normal fibroblast cells to produce progerin.

Extensive alternative splicing events occur during cell senescence. Next, we asked whether telomere dysfunction induces a broader set of alternative splicing changes, beyond the effects on *LMNA*. To monitor global effects on alternative splicing, we used the human Exon 10ST array, a splicing-sensitive microarray with probes targeted to individual exons or exon junctions, although it is not designed to detect use of the progerin cryptic splice site. This design allowed us to detect RNA isoforms expressed while simultaneously profiling gene expression. The expression level of each exon on each array was detected independently and analyzed using XRAY microarray analysis software.

The profiles of exon usage were compared between the same fibroblast lines with either long or short telomeres (group A) and between passage-matched fibroblasts where no significant variations in telomere length were present (group B), as controls (Figure 7A). Group A included 2 comparisons between early- and late-passage normal fibroblast cells (groups A1 and A2) and 2 comparisons between passage-matched human TERT–immortalized and nonimmortalized cells (groups A3 and A4). Group B comparisons included 4 comparisons between passage-matched normal and HGPS fibroblasts. Using a false discovery rate (FDR) threshold of 0.01, we identified numerous changes in gene expression in each comparison, even between the passage-matched fibroblasts from 2 normal individuals (data not shown). Surprisingly, changes in alternative splicing were much more prominent in group A, in which significant telomere shortening had occurred (Figure 7A and Supplemental Table 1). Between 10% and 50% of the genes showing changes in alternative splicing also exhibited differential regulation of gene expression (Figure 7A), which suggested distinct but also partially overlapping programs of transcriptional and posttranscriptional regulation. An overlap of 82 genes was observed in the 4 comparisons of group A (Figure 7B and Supplemental Table 2), which implies that 1 or more common regulatory pathways might be activated in these cells by shortening of telomeres. Statistical analysis (see Methods) indicated that the overlap of genes showing altered expression and altered splicing *within* all 4 group A sets was not significant ($P > 0.75$); however, the overlap of 82 genes with altered splicing *between* the 4 sets was highly significant ($P < 0.0001$). We were unable to identify any obvious pattern or sequence motifs in the set of genes that showed alternative splicing in the presence of telomere shortening.

In an attempt to address the functional relevance of these differentially spliced genes induced by changes in telomere length, gene

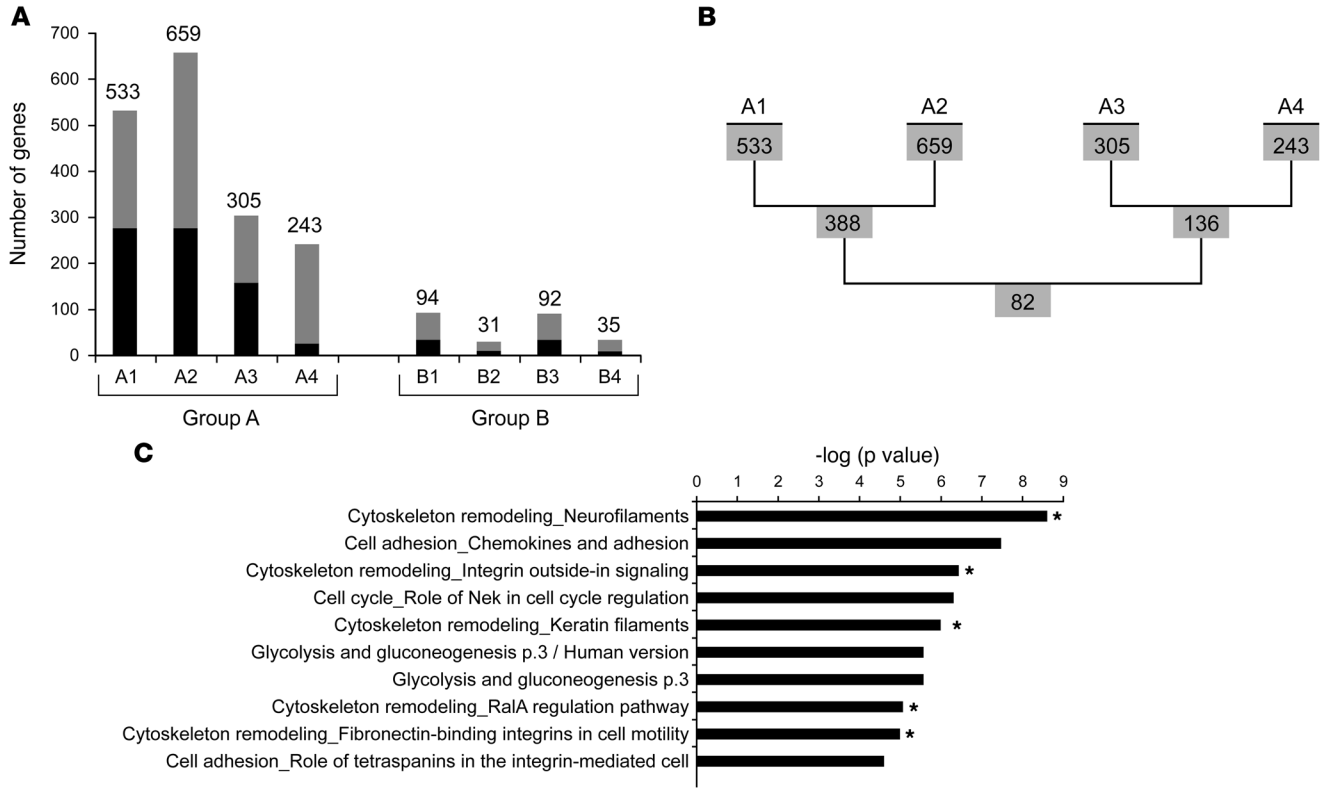

Figure 7

Extensive alterations in alternative splicing occur as cells senesce. (**A**) Number of genes that showed significant changes in alternative splicing in each indicated comparison. Gray, genes that exhibited changes only in alternative splicing; black, genes that exhibited changes both in alternative splicing and in gene expression. Group A included binary comparisons between normal fibroblasts before and after senescence: A1, p34 vs. p52 for normal fibroblast AG06299; A2, p7 vs. p22 for normal fibroblast HGFDFN168; A3, normal vs. human TERT–immortalized fibroblast HGFDFN090 at p6; A4, human TERT–immortalized vs. nonimmortalized normal fibroblast AG08398 at p8. Group B compared passage-matched fibroblasts where no significant variations in telomere length are present: B1, HGPS fibroblast HGADFN167 at p15 vs. HGPS fibroblast HGADFN003 at p16; B2, normal fibroblast HGFDFN168 at p14 vs. normal fibroblast HGFDFN090 at p14; B3, HGPS fibroblast HGADFN167 at p15 vs. age-matched normal fibroblast AG08470 at p14; B4, HGPS fibroblast HGADFN003 at p16 vs. age-matched normal fibroblast AG08470 at p14. (**B**) There were 82 overlapping genes among the 4 lists of genes in group A. (**C**) GO analysis (sorted by process networks) of the 82 overlapping genes in **B**. The top 10 enriched categories are shown; cytoskeleton-related categories are denoted with asterisks.

ontology (GO) enrichment analyses (see Methods) were carried out for these 82 common genes, using the complete set of genes covered by the exon microarray as a reference. Interestingly, among the top 10 most overrepresented categories, 5 were related to cytoskeleton organization and function, including the genes regulating intermediate filaments and microtubules, such as actin, fibronectin, vimentin, and tubulin (Figure 7C). These results indicate that cellular senescence induces extensive changes in alternative splicing in multiple genes and suggest a potential role of differential splicing in cytoskeleton reorganization during cellular aging.

Discussion

Considerable progress has been made in understanding the connection between HGPS and normal aging. In 2006, Scaffidi et al. first showed that the normal *LMNA* sequence could produce progerin at a low level in normal individuals, potentially implicating progerin in normal physiological aging (35). With a progerin-specific antibody, we previously demonstrated that the progerin-expressing cells from normal individuals mimic some aspects of HGPS cells, further supporting the idea that the premature aging disease HGPS and normal aging may share a common cellular and molecular basis (26). Furthermore, a recent analysis has shown that levels of *progerin* mRNA transcript increase in late-passage cells in vitro (37), and progerin protein accumulates with age in vivo in normal individuals (36). However, the cause-and-effect relationship between progerin production and aging has not been clear.

In this study, we applied a splice reporter assay that permits observation of the immediate effects of cell passage or donor age on the activation of the progerin cryptic splice site in *LMNA*. In normal fibroblasts, we showed that this cryptic site was increasingly activated as cells reached later cellular passage numbers. Thus, cellular senescence correlated with enhanced progerin production. No obvious correlation was found, however, between progerin production and donor age. One potential explanation is that the cells capable of growing in culture from a skin biopsy are relatively early in their in vivo passage number, regardless of the subject's chronological age (39).

We further showed that the fibroblast cells that used the *LMNA* cryptic splice site had shorter telomeres and exhibited high senescence-associated β-gal (SA–β-gal) activity. The finding that most of

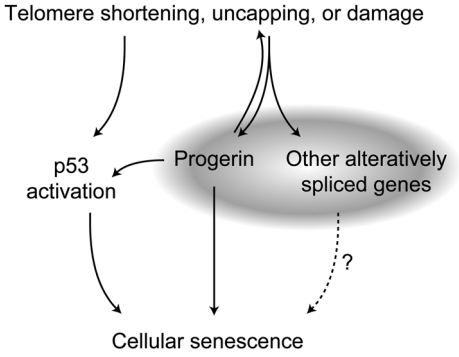

Figure 8
Proposed model of senescence. Previous work has shown that dysfunctional telomeres activate p53; apparently, so does progerin in HGPS cells. However, as shown in the present study, telomere shortening, uncapping, or damage in normal cells also triggers alternative splicing of a suite of genes, including production of *progerin* mRNA and progerin protein. These changes, in turn, may make a significant contribution to cellular senescence. The very recent report from Benson et al. (47) suggests that the signaling from telomeres to progerin may represent a bidirectional prosenescence feedback loop.

the cells with activated progerin splicing were senescent suggests a possible role of the cryptic splice reporter for progerin as a biomarker for cellular senescence. Previously, McClintock et al. found that progerin-expressing normal cells in skin biopsies were restricted to dermal fibroblasts and terminally differentiated keratinocytes and suggested that the population of progerin-expressing fibroblasts in skin might characterize a possible terminal differentiation phenotype in vivo (36). While distinct, both cellular senescence and terminal differentiation share some common characteristics including cell-cycle arrest, flattened and enlarged cell morphology, and changes in chromatin organization and in gene expression (36). It is possible that the progerin splicing events in cultured cells in vitro partially recapitulate the process of progerin production in normal tissues in vivo, and it will be interesting to determine the telomere length in those progerin-expressing cells in skin tissues.

In support of the notion that progerin production is selectively induced in senescent cells with short dysfunctional telomeres, we showed that *progerin* mRNA was essentially absent in immortalized cells. Significantly, human TERT immortalization experiments in primary healthy fibroblast cells revealed that the forced elongation of telomeres suppressed progerin production, which suggests that telomere shortening lies upstream of activation of the cryptic splice site. This conclusion is consistent with the observation that progerin production was not altered in oncogene-induced cellular senescence, in which telomere shortening was not involved. In further support of this model, an elevated amount of progerin was observed in DC fibroblast cells carrying a null *TERT* mutation. Notably, cells expressing TRF2$^{\Delta B\Delta M}$, which induces uncapping of telomeres, showed substantial upregulation of progerin production. Taken together, these observations support the conclusion that shortened or uncapped telomeres act as an upstream signal to activate progerin production in primary fibroblast cells.

Is the reverse pathway also present, i.e., does expression of progerin affect telomere maintenance? The answer to this question has been controversial in the literature. A previous study reported that one-third of the independent isolated fibroblast clones from HGPS patients fail to immortalize despite the exogenous expression of telomerase, which suggests that the growth arrest in HGPS confers resistance to telomerization (44). Another report indicated that telomerase failed to protect progerin-induced DNA damage (45). However, Decker et al. reported shortened telomeres in HGPS fibroblasts, although their finding was limited to late-passage HGPS fibroblasts, where telomere attrition may well have been on the basis of cell passage number rather than being specific for HGPS (46). Most recently, a report by Benson et al. showed that exogenous expression of progerin in human diploid fibroblasts rapidly induces telomere aggregation, appearance of DNA-damage signals at telomeres, and chromosomal aberrations. Importantly, these effects were abolished by telomerase expression (47). Using quantitative telomere PNA-FISH in HGPS fibroblasts, we found no clear evidence of shortened telomeres compared with passage-matched normal fibroblasts (data not shown). Similarly, we found that the telomere length in vascular smooth muscle cells derived from a transgenic mouse model of HGPS was no different from that in nontransgenic control mice (data not shown). In support of the conclusion that progerin's effect on telomeres is independent of shortening of the telomeric DNA, Benson et al. (47) indicated that progerin induces rapid telomere dysfunction well before telomere attrition would be detectable. Therefore, we suggest that progerin induces an acute DNA damage response at telomeres — perhaps on the basis of well-established effects of progerin on disrupting heterochromatin structure (21) — that leads to deprotection of the telomeric 3′ overhang.

Cellular senescence reflects a complex process of gradual deterioration of the molecular components, checkpoints, and cellular structures. Inspired by the progerin results, we hypothesized that alternative splicing, a key pre-mRNA processing step, might be more broadly influenced by senescence. Using splicing-sensitive exon microarrays, we showed that not only *LMNA* splicing was affected by short telomeres, but a significant number of other genes were also affected. Interestingly, GO analysis further demonstrated that the most overrepresented categories in this set of differentially spliced genes were related to cytoskeleton function. This finding may connect with the longstanding observation that senescent cells demonstrate characteristic changes in cytoskeleton organization, including cell shapes, cell adhesion, and cell mobility. Previous studies reported that fibronectin (48), a cell adhesion protein, and vimentin (49, 50), an intermediate filament protein, are alternatively spliced in senescent cells. Both were identified in our analysis, as were other cytoskeleton-related proteins, such as actin and tubulin. Our studies present what we believe to be the first systematic genome-wide analysis of alternative splicing during cellular senescence and suggest a significant potential role of differential splicing in cytoskeleton reorganization during cellular aging.

To summarize, we demonstrated that progressive telomere loss in normal cells acted as an upstream signal to activate the cryptic splice site in *LMNA* to produce progerin as well as to induce alternative splicing of a number of other genes. Telomere-induced senescence has previously been primarily attributed to the activation of the tumor suppressor p53 (11). Interestingly, in HGPS cells, progerin-induced senescence has also been partially linked to the activation of p53 (51). Taken together, our data suggest a more complex model: in addition to activation of p53, progressive telomere shortening triggers alternative splicing of a suite of genes, including production of *progerin* mRNA and progerin protein. These changes, in turn, contribute to cellular senescence

(Figure 8). The recent report from Benson et al. (47) adds another potential feature to this mechanism — a positive feedback loop between telomeres and progerin.

The specific signaling pathway from dysfunctional telomeres to the spliceosome machinery remains undefined. An attractive hypothesis is that certain telomere-binding/capping proteins are released from telomere ends when telomeres are progressively shortened or damaged, and then influence spliceosome function in senescent cells. One potential candidate for carrying out this function is the shelterin complex, consisting of 6 telomere-binding proteins: TRF1, TRF2, POT1, TIN2, Rap1, and TPP1. Acting together with DNA repair factors, these proteins protect telomere ends by forming a specialized complex that masks the telomeres from being seen as sites of DNA damage (4). The released shelterin proteins could potentially act as signal transducers for alternative splicing in senescent cells. Other factors that may directly influence alternative splicing would include the heterogeneous nuclear ribonucleoproteins (hnRNPs), which bind to both RNA and single-stranded telomere DNA. In fact, hnRNPs have been suggested to participate in the posttranscriptional processing of precursor mRNA (52). Moreover, there is evidence suggesting that the single-stranded DNA binding activity of 2 hnRNPs, A1 and A2, is reduced in senescent cells (53, 54). Given the finding on the activation of extensive alternative splicing in senescent cells, it will be of great interest to determine whether shelterin, hnRNPs, and/or other telomere-binding proteins may play a role in pre-mRNA splicing in cellular aging. In summary, the present studies uncover what we believe to be a novel signaling pathway for cellular senescence and further enhance the conclusion that the study of HGPS can provide critical clues to the normal aging process.

Methods

Cell culture. Primary human dermal fibroblasts were cultured under 5% CO_2 (balanced by ambient air) in MEM (Gibco; Invitrogen) supplemented with 15% FBS (Invitrogen) plus 2 mM L-glutamine. The primary fibroblast cell lines used in our studies included AG06299 (normal), AG08470 (normal), AG07306 (normal), AG08048 (normal), AG06277 (normal), AG09838 (normal), and AG09602 (normal) from Coriell Cell Repositories and HGADFN167 (HGPS), HGADFN003 (HGPS), HGFDFN168 (normal), and HGFDFN090 (normal) from the Progeria Research Foundation. See Supplemental Table 3 for detailed information for each cell line. The hTERT-HGFDFN090 and hTERT-AG09838 stable fibroblast cell lines were generated and provided by T. Glover (University of Michigan, Ann Arbor, Michigan, USA). Each cell passage was defined as a 3-fold split. Normal fibroblasts typically grew for about 30 passages, and HGPS fibroblasts grew 15–20 passages, under the culturing condition.

The human coronary vascular SMCs were cultured in SmGM-2 medium (Lonza). In addition, 2 normal primary B lymphocyte cell lines (AG11506 and AG09393) were obtained from Coriell Cell Repositories. The immortalized cells HeLa, HepG2, Mcf7, and 293T were cultured in DMEM (Gibco; Invitrogen) supplemented with 10% heat-inactivated FBS (Gibco; Invitrogen).

Primary DC fibroblast cells were provided from skin biopsies using standard methods by M. Armanios (Johns Hopkins University School of Medicine, Baltimore, Maryland, USA). Briefly, the skin biopsy was minced and grown in MEM with Earle's and 20% fetal bovine serum. After first passage, cells were maintained in complete media containing 10% serum. The study was approved by the Johns Hopkins Institutional Review Board.

Splicing reporter construct. The original splice reporter construct was provided by T. Misteli (National Cancer Institute, NIH, Bethesda, Maryland, USA). To subclone the splicing reporter into the pIRES-DsRed-Expression 2 vector, the pPRO reporter previously described (35) was PCR amplified using the following primers: forward, CCGCTCGAGGTACGGCTCTCATCAACTCC; reverse, CCGCTCGAGTTACTTGTACAGCTCGTC. The PCR product was subsequently cloned into the XhoI site of pIRES-DsRed-Expression 2 vector, and the correct orientation of the insert was determined by sequencing.

Transfection. All transient transfections with the progerin splicing reporter in the primary fibroblasts were performed using the Amaxa nucleofection device and nucleofector kits for adult human–dermal fibroblasts (NHDF; Lonza) according to the manufacturer's instructions.

Antibodies. The antibodies used in the study included a rabbit polyclonal antibody against progerin (provided by K. Djabali, Columbia University, New York, New York, USA), mouse anti–lamin A/C (MAB3211; Chemicon), mouse anti-tubulin (DM1α; Sigma-Aldrich), rabbit anti-GFP (Abcam), and mouse anti-GAPDH (Abcam).

FACS. Primary fibroblasts transfected with the progerin splicing reporter were excited at 488 nm and sorted with a FACSAria machine (BD) according to the manufacturer's instructions.

RNA isolation, reverse transcription, qRT-PCR, and data analysis. Cells were harvested at approximately 75% confluence. RNA for each sample was isolated with the Qiagen RNAesy kit according to the manufacturer's instructions. RNA was reverse transcribed using the superscript III kit (Invitrogen) according to the manufacturer's instructions. qRT-PCR was performed to measure expression of *progerin*, *LMNA*, *TERT*, and *ACTB*. All reactions were carried out at least in triplicate on an Applied Biosystems 7900HT Fast Real-Time PCR System using SYBR Green mix (Qiagen) according to the manufacturer's instructions. Reaction conditions were as follows: 1 cycle of 2 minutes at 50°C; 1 cycle of 10 minutes at 95°C; and 40 cycles of 15 seconds at 95°C, 15 seconds at 58°C, and 30 seconds at 72°C. Primers for TERT and β-actin were obtained from R&D and Ambion, respectively. The sequence of the forward primer for amplifying progerin/lamin A is GCAACAAGTCCAATGAGGACCA. The progerin- and lamin A–specific reverse primers were designed according to amplification-refractory mutation system strategy, by introducing a mutation at the penultimate base to increase specificity. The progerin-specific primer sequence is CATGATGCTGCAGTTCTGGGGGCTCTGGAC, and that for lamin A is CATGATGCTGCAGTTCTGGGGGCTCTGGAT. To normalize for mRNA input in each reaction, the relative expression values for *LMNA*, *progerin*, or *TERT* were normalized to the mean values of *ACTB*. Expression values for each gene were expressed as mean ± SD of experimental triplicates.

Quantitative telomere PNA-FISH analysis. FISH was performed with the Telomere PNA Kit (Dako) according to the manufacturer's protocol. Confocal images were acquired at room temperature using a Zeiss LSM 510 NLO Meta system mounted on a Zeiss Axiovert 200M microscope with an oil immersion Plan-Apochromat ×63/1.4 differential image contrast objective lens. Excitation wavelengths of 488 nm (4%), 561 nm (7%), and 740 nm (3%) were used for detection of the FITC-tagged telomeric probe, the Cy3-tagged telomeric probe, and DAPI, respectively. Fluorescent emissions were collected in a BP 500- to 550-nm IR blocked filter, LP 575-nm filter, and BP 390- to 465-nm IR blocked filter, respectively. All pinholes were set with a range from 1.21 to 1.39 Airy units, which correspond to an optical slice of 1.0 μm (excluding the DAPI channel, for which a multiphoton laser was used). All confocal images were of frame size 512 pixels × 512 pixels, scan zoom 2, and were line averaged 8 times. Confocal images were postprocessed using MediaCybernetics Image-Pro Plus software (version 6.3). Every image was processed using a custom macro designed to calibrate, filter (Gaussian), segment (touching nuclei or nuclei touching the image border were not included), outline the nuclei, count, and record measurements. Measurements included nucleus area (μm²) and fluorescent intensity

(minimum, maximum, mean, SD, and sum) measurements. Nuclei outlines were obtained using DAPI staining as the template, then propagating that outline throughout the FITC and Spectrum Orange channels. At least 20–30 randomly chosen nuclei were processed per cell line.

Immunofluorescence analysis. Immortalized cells or primary fibroblasts grown on chamber slides (Nunc) were fixed either with 4% formaldehyde in PBS for 20 minutes at room temperature followed by a 5-minute treatment with 0.5% Triton-X 100 in PBS, or with methanol/Acetone (1:1) at –20°C as described previously (26). The fixed cells were rinsed with PBS and blocked with 10% horse serum and 4% BSA in PBS for 30 minutes. Cells were then incubated for 1 hour with the primary antibodies diluted in blocking solution. The secondary antibodies were Alexa 488– or Alexa 594–conjugated donkey anti-rabbit or donkey anti-mouse IgG antibodies (Invitrogen). All samples were also counterstained with DAPI (Vector Laboratories). Cells were observed with a LSM510 or LSM710 confocal microscope (Zeiss) or an Axioplan fluorescence microscope (Zeiss).

SA–β-gal activity assay. Subconfluent primary fibroblasts grown on chamber slides (Nunc) were fixed in 3% formaldehyde and stained overnight at 37°C with X-gal buffered with sodium phosphate at pH 6.0 in the presence of potassium ferrocyanide and potassium ferricyanide as described previously (55).

Exon microarray processing and analysis. Total RNAs were prepared according to Affymetrix protocols (Affymetrix). RNA quality and quantity was ensured using the Bioanalyzer (Agilent) and NanoDrop (Thermo Scientific), respectively. For RNA labeling, 1 μg total RNA was used in conjunction with the Affymetrix-recommended protocol for GeneChip WT Sense Target Labeling. The total RNA was first subjected to a ribosomal RNA reduction using the Invitrogen RiboMinus Transcriptome Isolation Kit. The remaining RNA was then reverse transcribed in the presence of dT7N6 primers to generate cDNA. An in vitro transcription was then performed, and the resulting cRNA was purified. A first-strand cDNA was generated form the cRNA in the presence of dUTPs. After RNA hydrolysis, the single-stranded cDNA was fragmented and end-labeled with biotin. The hybridization cocktail containing the fragmented and biotin-labeled cDNAs were hybridized to the Affymetrix GeneChip Human Exon 1.0 ST Array. The chips were washed and stained by the Affymetrix Fluidics Station using the standard format and protocols as described by Affymetrix. The probe arrays were stained with streptavidin phycoerythrin solution (Invitrogen) and enhanced using an antibody solution containing 0.5 mg/ml biotinylated anti-streptavidin (Vector Laboratories). An Affymetrix Gene Chip Scanner 3000 was used to scan the probe arrays. Gene expression intensities were calculated using Affymetrix Expression Console software, and .cel files were generated. Each sample was processed in technical triplicates. Data were deposited in NCBI Gene Expression Omnibus (accession no. GSE28863; http://www.ncbi.nlm.nih.gov/geo/query/acc.cgi?acc=GSE28863).

All exon array analysis was performed using XRAY microarray analysis software (version 3.9). Full quantile normalization was performed to minimize technical variance within the data. Only core probe sets (corresponding to high-quality genomic features like RefSeq or Ensembl transcripts) were considered for analysis. Probes with GC counts less than 6 and greater than 17 were filtered from the analysis, and the probe scores were transformed by taking natural logarithm of 0 plus the probe score. Background correction for each probe score was carried out by subtracting the median expression score of background probes with similar GC content. The expression score for a probe set was calculated as the median of all probes within the set, and probe sets with fewer than 3 probes were filtered from further analysis. Mixed model nested ANOVA was used to identify genes with statistically significant group-specific gene expression or alternative splicing. FDR method was used to correct for multiple testing, and FDR of 1.00 or less was considered significant for both differential alternative splicing and gene expression tests. A P value threshold of 0.001 was used to reject the null hypothesis that the average of group expression is not above background. P value filters were also applied to group expression levels for each gene to reduce false positives for alternative splicing. Quality control diagnostics produced for each array before and after normalization proved the good quality of arrays. GO enrichment analysis for the gene lists was carried out using MetaCore (GeneGo). Categories with an FDR of 0.05 or less were considered statistically significant.

To assay the statistical significance of the overlap between the genes showing altered expression and altered splicing, we randomly selected transcripts/genes from the final list of probes considered for the analysis. For example, for group A1, we randomly selected 3,900 of approximately 7,900 total genes and 533 of approximately 89,000 total transcripts represented in the final probe list. We then determined the number of overlaps between these randomly selected genes and transcripts. This was done 10,000 times to generate a distribution of the random overlaps between genes and transcripts for the group A1 set. The overlap of genes showing altered expression and altered splicing *within* all 4 group A sets was not statistically significant ($P > 0.75$). A similar analysis was carried out to determine the statistical significance of overlapping 82 genes among the 4 group A sets. In this case, we randomly selected a defined number of transcripts for each of the 4 group A sets and looked for overlap among them. For example, we randomly pulled 533 transcripts from group A1, 659 from group A2, 305 from group A3, and 243 from group A4 and determined the number of shared transcripts. We repeated this analysis 10,000 times to generate a distribution of how often the sets of alternatively spliced genes overlapped at random. In this case, the overlap of 82 genes with altered splicing *between* the 4 sets was found to be highly significant ($P < 0.0001$).

Sequencing of TERT in DC cells. Genomic DNA from JH-1 and JH-2 lines was prepared using DNeasy Blood and Tissue Kit (Qiagen). The DNA fragment that flanks the K902N mutation in *TERT* was PCR amplified with the following primers: forward, CGGGCTGCTCCTGCGTTTGGTG; reverse, ACATCCCTGCGTTCTTGGCTTTCA. The amplified PCR products were sequenced by ACGT Inc.

Retrovirus-mediated gene transfer. Retroviral packaging BOSC 23 cells (6×10^6; ATCC) were plated in a 25-cm dish, incubated for 24 hours, and then transfected by Fugene 6 (Promega) with 30 μg retroviral plasmids. The retroviral plasmids pBABE-puro H-rasV12, pBABE-puro control, and pLPC- TRF2 (WT and mutant) were obtained from Addgene. After 60 hours, the retrovirus-containing medium was filtered (0.45-μm filter; Millipore), concentrated 50-fold (from 25 ml to 500 μl), and titrated. The target normal fibroblasts were plated at 70%–80% confluence in a 10-cm dish the night before infection. Each infection used 100 μl of the concentrated virus (MOI 0.5) supplemented with 5 μg/ml polybrene (Sigma-Aldrich). The infected normal fibroblast cells were selected in media containing 2 μg/ml puromycin for 5 days after infection and were then grown in regular media for an additional 6 days for analysis.

Statistics. Unless otherwise specified, results are presented as mean ± SD. Data were analyzed using 2-tailed Student's t test, and a P value less than 0.05 was considered significant.

Acknowledgments

We thank Stephen Wincovitch and Amalia Dutra for support of the quantitative telomere PNA-FISH experiments, Stacie Anderson for support of the FACS analysis, Abdel Elkahloun for support of the exon array experiment, Tyra Wolfsberg for help with GO analysis, Darryl Leja for help with figures, Thomas Misteli for the original splice reporter construct, Thomas Glover for the human TERT–immortalized fibroblast cell lines, Mary Armanios for the DC fibroblast cell lines and helpful discussions, Samir Kelada for

statistical help, and Karima Djabali for the anti-progerin antibody. This work was supported by NIA/NIH grant R00AG029761 (to K. Cao) and by the intramural program of the National Human Genome Research Institute (to F.S. Collins).

Address correspondence to: Francis S. Collins, National Institutes of Health, One Center Drive, Room 126, Bethesda, Maryland 20892-0148, USA. Phone: 301.496.2433; Fax: 301.402.2700; E-mail: Francis.Collins@nih.gov.

Received for publication May 2, 2010, and accepted in revised form May 4, 2011.

Elizabeth G. Nabel's present address is: Brigham and Women's Hospital, Boston, Massachusetts, USA.

1. Hayflick L. Intracellular determinants of cell aging. *Mech Ageing Dev*. 1984;28(2–3):177–185.
2. Jeyapalan JC, Sedivy JM. Cellular senescence and organismal aging. *Mech Ageing Dev*. 2008; 129(7–8):467–474.
3. Olovnikov AM. Telomeres, telomerase, and aging: origin of the theory. *Exp Gerontol*. 1996; 31(4):443–448.
4. de Lange T. Shelterin: the protein complex that shapes and safeguards human telomeres. *Genes Dev*. 2005;19(18):2100–2110.
5. Harley CB, Futcher AB, Greider CW. Telomeres shorten during ageing of human fibroblasts. *Nature*. 1990;345(6274):458–460.
6. Blackburn EH. Structure and function of telomeres. *Nature*. 1991;350(6319):569–573.
7. Greider CW. Telomere length regulation. *Annu Rev Biochem*. 1996;65:337–365.
8. Blasco MA. Mammalian telomeres and telomerase: why they matter for cancer and aging. *Eur J Cell Biol*. 2003;82(9):441–446.
9. Bodnar AG, et al. Extension of life-span by introduction of telomerase into normal human cells. *Science*. 1998;279(5349):349–352.
10. Reddel RR. A reassessment of the telomere hypothesis of senescence. *Bioessays*. 1998;20(12):977–984.
11. Shawi M, Autexier C. Telomerase, senescence and ageing. *Mech Ageing Dev*. 2008;129(1–2):3–10.
12. Serrano M, Lin AW, McCurrach ME, Beach D, Lowe SW. Oncogenic ras provokes premature cell senescence associated with accumulation of p53 and p16INK4a. *Cell*. 1997;88(5):593–602.
13. Capell BC, Collins FS. Human laminopathies: nuclei gone genetically awry. *Nat Rev Genet*. 2006;7(12):940–952.
14. Eriksson M, et al. Recurrent de novo point mutations in lamin A cause Hutchinson-Gilford progeria syndrome. *Nature*. 2003;423(6937):293–298.
15. Goldman RD, Gruenbaum Y, Moir RD, Shumaker DK, Spann TP. Nuclear lamins: building blocks of nuclear architecture. *Genes Dev*. 2002;16(5):533–547.
16. Dechat T, Adam SA, Goldman RD. Nuclear lamins and chromatin: When structure meets function. *Adv Enzyme Regul*. 2009;49(1):157–166.
17. Dechat T, et al. Nuclear lamins: major factors in the structural organization and function of the nucleus and chromatin. *Genes Dev*. 2008;22(7):832–853.
18. Merideth MA, et al. Phenotype and course of Hutchinson-Gilford progeria syndrome. *N Engl J Med*. 2008;358(6):592–604.
19. De Sandre-Giovannoli A, et al. Lamin a truncation in Hutchinson-Gilford progeria. *Science*. 2003; 300(5628):2055.
20. Olive M, et al. Cardiovascular pathology in hutchinson-gilford progeria: correlation with the vascular pathology of aging. *Arterioscler Thromb Vasc Biol*. 2010; 30(11):2301–2309.
21. Goldman RD, et al. Accumulation of mutant lamin A causes progressive changes in nuclear architecture in Hutchinson-Gilford progeria syndrome. *Proc Natl Acad Sci U S A*. 2004;101(24):8963–8968.
22. Shumaker DK, et al. Mutant nuclear lamin A leads to progressive alterations of epigenetic control in premature aging. *Proc Natl Acad Sci U S A*. 2006;103(23):8703–8708.
23. Ly DH, Lockhart DJ, Lerner RA, Schultz PG. Mitotic misregulation and human aging. *Science*. 2000;287(5462):2486–2492.
24. Csoka AB, et al. Genome-scale expression profiling of Hutchinson-Gilford progeria syndrome reveals widespread transcriptional misregulation leading to mesodermal/mesenchymal defects and accelerated atherosclerosis. *Aging Cell*. 2004;3(4):235–243.
25. Liu B, et al. Genomic instability in laminopathy-based premature aging. *Nat Med*. 2005;11(7):780–785.
26. Cao K, Capell BC, Erdos MR, Djabali K, Collins FS. A lamin A protein isoform overexpressed in Hutchinson-Gilford progeria syndrome interferes with mitosis in progeria and normal cells. *Proc Natl Acad Sci U S A*. 2007;104(12):4949–4954.
27. Dechat T, et al. Alterations in mitosis and cell cycle progression caused by a mutant lamin A known to accelerate human aging. *Proc Natl Acad Sci U S A*. 2007;104(12):4955–4960.
28. Varga R, et al. Progressive vascular smooth muscle cell defects in a mouse model of Hutchinson-Gilford progeria syndrome. *Proc Natl Acad Sci U S A*. 2006;103(9):3250–3255.
29. Sinensky M, Fantle K, Trujillo M, McLain T, Kupfer A, Dalton M. The processing pathway of prelamin A. *J Cell Sci*. 1994;107(pt 1):61–67.
30. Yang SH, et al. Blocking protein farnesyltransferase improves nuclear blebbing in mouse fibroblasts with a targeted Hutchinson-Gilford progeria syndrome mutation. *Proc Natl Acad Sci U S A*. 2005; 102(29):10291–10296.
31. Capell BC, et al. Inhibiting farnesylation of progerin prevents the characteristic nuclear blebbing of Hutchinson-Gilford progeria syndrome. *Proc Natl Acad Sci U S A*. 2005;102(36):12879–12884.
32. Capell BC, et al. A farnesyltransferase inhibitor prevents both the onset and late progression of cardiovascular disease in a progeria mouse model. *Proc Natl Acad Sci U S A*. 2008;105(41):15902–15907.
33. Yang SH, et al. A farnesyltransferase inhibitor improves disease phenotypes in mice with a Hutchinson-Gilford progeria syndrome mutation. *J Clin Invest*. 2006;116(8):2115–2121.
34. Fong LG, et al. A protein farnesyltransferase inhibitor ameliorates disease in a mouse model of progeria. *Science*. 2006;311(5767):1621–1623.
35. Scaffidi P, Misteli T. Lamin A-dependent nuclear defects in human aging. *Science*. 2006; 312(5776):1059–1063.
36. McClintock D, et al. The mutant form of lamin A that causes Hutchinson-Gilford progeria is a biomarker of cellular aging in human skin. *PLoS ONE*. 2007; 2(12):e1269.
37. Rodriguez S, Coppede F, Sagelius H, Eriksson M. Increased expression of the Hutchinson-Gilford progeria syndrome truncated lamin A transcript during cell aging. *Eur J Hum Genet*. 2009;17(7):928–937.
38. Scaffidi P, Misteli T. Good news in the nuclear envelope: loss of lamin A might be a gain. *J Clin Invest*. 2006;116(3):632–634.
39. Cristofalo VJ, Allen RG, Pignolo RJ, Martin BG, Beck JC. Relationship between donor age and the replicative lifespan of human cells in culture: a reevaluation. *Proc Natl Acad Sci U S A*. 1998;95(18):10614–10619.
40. Moss SF, et al. Decreased and aberrant nuclear lamin expression in gastrointestinal tract neoplasms. *Gut*. 1999;45(5):723–729.
41. Munro J, Barr NI, Ireland H, Morrison V, Parkinson EK. Histone deacetylase inhibitors induce a senescence-like state in human cells by a p16-dependent mechanism that is independent of a mitotic clock. *Exp Cell Res*. 2004;295(2):525–538.
42. Armanios M, et al. Haploinsufficiency of telomerase reverse transcriptase leads to anticipation in autosomal dominant dyskeratosis congenita. *Proc Natl Acad Sci U S A*. 2005;102(44):15960–15964.
43. Jacobs JJ, de Lange T. Significant role for p16INK4a in p53-independent telomere-directed senescence. *Curr Biol*. 2004;14(24):2302–2308.
44. Wallis CV, Sheerin AN, Green MH, Jones CJ, Kipling D, Faragher RG. Fibroblast clones from patients with Hutchinson-Gilford progeria can senesce despite the presence of telomerase. *Exp Gerontol*. 2004; 39(4):461–467.
45. Scaffidi P, Misteli T. Lamin A-dependent misregulation of adult stem cells associated with accelerated ageing. *Nat Cell Biol*. 2008;10(4):452–459.
46. Decker ML, Chavez E, Vulto I, Lansdorp PM. Telomere length in Hutchinson-Gilford progeria syndrome. *Mech Ageing Dev*. 2009;130(6):377–383.
47. Benson EK, Lee SW, Aaronson SA. Role of progerin-induced telomere dysfunction in HGPS premature cellular senescence. *J Cell Sci*. 2010; 123(pt 15):2605–2612.
48. Magnuson VL, et al. The alternative splicing of fibronectin pre-mRNA is altered during aging and in response to growth factors. *J Biol Chem*. 1991; 266(22):14654–14662.
49. Nishio K, Inoue A. Senescence-associated alterations of cytoskeleton: extraordinary production of vimentin that anchors cytoplasmic p53 in senescent human fibroblasts. *Histochem Cell Biol*. 2005;123(3):263–273.
50. Nishio K, Inoue A, Qiao S, Kondo H, Mimura A. Senescence and cytoskeleton: overproduction of vimentin induces senescent-like morphology in human fibroblasts. *Histochem Cell Biol*. 2001; 116(4):321–327.
51. Varela I, et al. Accelerated ageing in mice deficient in Zmpste24 protease is linked to p53 signalling activation. *Nature*. 2005;437(7058):564–568.
52. Mayeda A, Munroe SH, Caceres JF, Krainer AR. Function of conserved domains of hnRNP A1 and other hnRNP A/B proteins. *EMBO J*. 1994; 13(22):5483–5495.
53. Zhu D, Xu G, Ghandhi S, Hubbard K. Modulation of the expression of p16INK4a and p14ARF by hnRNP A1 and A2 RNA binding proteins: implications for cellular senescence. *J Cell Physiol*. 2002;193(1):19–25.
54. Hubbard K, et al. Alteration of DNA and RNA binding activity of human telomere binding proteins occurs during cellular senescence. *Exp Cell Res*. 1995;218(1):241–247.
55. McClintock D, Gordon LB, Djabali K. Hutchinson-Gilford progeria mutant lamin A primarily targets human vascular cells as detected by an anti-Lamin A G608G antibody. *Proc Natl Acad Sci U S A*. 2006; 103(7):2154–2159.